Anal. Bioanal. Electrochem., Vol. 10, No. 12, 2018, 1548-1561

Analytical & Bioanalytical Electrochemistry

2018 by CEE
www.abechem.com

Full Paper

Design of Experiments Methodology to Investigate Methanol Electrooxidation on Pt Nanoparticles Supported Novel Functionalized Reduced Graphene Oxide

Mehri-Saddat Ekrami-Kakhki, Sedigheh Abbasi* and Nahid Farzaneh

Central Research Laboratory, Esfarayen University of Technology, Esfarayen, North Khorasan, Iran

*Corresponding Author, Tel.: 0583-7266531; Fax: 05837266534

E-Mail: s.abbasi@esfarayen.ac.ir; abasi_1362@yahoo.com

Received: 16 July 2018 / Received in revised form: 29 October 2018 / Accepted: 5 November 2018 / Published online: 31 December 2018

Abstract- Here, graphene oxide is synthesized and functionalized with methyl viologen and chitosan to be used as a novel catalyst support for Pt nanoparticles. The particle size and distribution of Pt nanoparticles are characterized by transmission electron microscope images. Pt nanoparticles with the mean particle size of 3.62 nm are dispersed on the support very uniformly. The catalytic activity of the prepared catalyst is investigated for methanol oxidation by cyclic voltammetry technique. The prepared catalyst showed very good catalytic activity for methanol oxidation. The experimental and statistical analyses are used to investigate the effect of mutual interaction between temperature and methanol concentration on anodic current density of methanol oxidation. The statistical analysis results reveals that the influence of temperature and methanol concentration as main factors and their reciprocal interactions are significant at α=0.05. Meanwhile, the results confirm that the response increases with both main factors. The enhancement of the anodic current density of methanol oxidation with temperature and methanol concentration is equal to 530.22% and 184.89%, respectively. Therefore, the effect of temperature on the response is higher than that of methanol concentration.

Keywords- Mutual interaction, Anodic current density, Methanol oxidation, Design of experiments

1. INTRODUCTION

Due to the global-energy crisis and serious environmental problems of using fossil fuels as energy sources, extensive studies have been done to find new energy conversion devices. Among different energy sources, direct methanol fuel cells (DMFCs) have attracted a lot of attention because of several advantages such as low pollution, low operating temperature, light weight, high conversion efficiency, and high power density [1,2]. To develop DMFCs, various catalytic materials have been studied for methanol oxidation reaction (MOR). Pt and Pt-based catalysts have been used as anode catalysts for methanol oxidation (MO) in DMFCs [3,4], and have exhibited very good activity for MO. However, easy poisoning of Pt catalysts with carbon monoxide, the intermediate of MO, limits their application in DMFCs [5]. Some factors such as preparation method and supporting materials affect the activity and performance of catalysts [6-8]. Supporting materials have a significant influence on stability, catalytic performance and dispersion of catalysts [9,10]. Many carbonaceous materials, such as carbon nanotubes [11], carbon nanofibers [12], mesoporous carbon [13,14] and graphene [15-17] have been used as support for Pt nanoparticles (PtNPs).

Graphene, the basic structure of all graphitic forms, has been used as a good support material for catalysts due to its remarkable thermal conductivity, high surface area, excellent mechanical properties and electronic conductivity [18, 19]. However, graphene has a great tendency for irreversible aggregation during synthesis process which reduces its specific surface area [20]. Graphene can be produced by chemical reduction of graphene oxide (GO). Reduced graphene oxide (RGO) has been used as support for dispersion of precious metal nanoparticles to improve their catalytic activities for MO [21]. However, reduction of GO decreases it's surface area. To overcome this problem, RGO is functionalized covalently and non-covalently. Non-covalent functionalization of graphene is preferable for catalyst supports and preserves their electronic characteristics [22-25]. Recently, Ma and coauthors used 1,1′-dimethyl-4,4′-bipyridinium dichloride (methyl viologen) for non-covalent functionalization of graphene [26].

In this work, graphene sheets are functionalized with methyl viologen (MV) accompanied by chitosan (CH) polymer to get MV-RGO-CH as catalyst support for electrooxidation of methanol. Chitosan is a biopolymer which is produced by deacetylation of chitin and has a strong affinity for transition metals [27]. Functionalization of reduced graphene oxide with methyl viologen accompanied by chitosan significantly improves the catalytic performance of Pt catalyst for MOR. Here, for the first time, a statistical analysis is done by design of experiments (DOE) to investigate the mutual interaction between temperature and methanol concentration on the anodic current density of MO on the prepared Pt catalyst. The statistical investigation of the main factors (such as temperature and methanol concentration), their combined effects and importance of each level have never been studied so far.

2. EXPERIMENTAL

2.1. Materials

Graphite powder (99.5%), H_2SO_4 (98%), HNO_3, $KMnO_4$ (99% for analysis), HCl (37%) and H_2O_2 (30%) are purchased from Merck. 1,1′-dimethyl-4,4′-bipyridinium dichloride (MV) 98% is purchased from Sigma Aldrich. H_2PtCl_6 and $NaBH_4$ 96% are prepared from Merck. Chitosan ([2-amino-2-deoxy-(1-4)-β-D-glucopyranose], medium molecular weight) is purchased from Fluka and dissolved in 1% acetic acid (glacial, 100%) from Merck. Methanol (CH_3OH, 99.2%) is purchased from Merck.

2.2. Preparation of methyl viologen-reduced graphene oxide (MV-RGO)

GO nanosheets are synthesized from graphite powder through a modified Hummers' method [28]. MV–RGO is synthesized through a simple method by chemical reduction of GO in the presence of MV [29]. Typically, 5 mL GO (11 mg mL^{-1}) is dispersed in 200 ml deionized water and sonicated for 1 h. MV (0.0178 g) is dissolved in 20 ml deionized water in a beaker and mixed with GO solution. Afterwards, 0.33 g $NaBH_4$ is added to the solution. The mixture is stirred for 24 h, centrifuged and washed with deionized water. Then, it is dried at 60 ˚C. MV-RGO is prepared.

2.3. Preparation of Pt/MV-RGO-CH catalyst

Pt/MV-RGO-CH nanocatalyst is prepared through the following steps: At first, a mixture of 1 mg MV-RGO, 17.5 ml deionized water and 2.5 ml CH is prepared. After being sonicated for 1 h, H_2PtCl_6 solution (0.00125 M) is prepared by adding 25 µl H_2PtCl_6 solution to the mixture. The mixture is stirred for 1 h. 50 µl $NaBH_4$ (3M) is added to the solution as reducing agent. After being stirred for 24 h, it is centrifuged to remove excess $NaBH_4$. Several centrifugation and washing processes are used to purify Pt-MV-RGO-CH catalyst. Finally, the prepared catalyst is dried at 60 ˚C for 12 h.

3. EXPERIMENTAL RESULTS AND DISCUSSION

3.1. Characterization of Pt/MV-RGO-CH catalyst

TEM image taken with a Philips CM120 transmission electron microscope with the resolution ~2.5 Å is used to determine the particle size and distribution of PtNPs on MV-RGO-CH support (Fig. 1). As shown in Fig. 1, PtNPs dispersed on MV-RGO-CH support are very uniform with very low agglomeration. The mean particle size of PtNPs was 3.62 nm. The uniform dispersion of PtNPs was due to the use of CH and MV as supporting material. CH has amino groups in its structure which are easily protonated to NH_3^+ in acidic solution.

The presence of the positively charged functional groups in MV-RGO and CH and their electrostatic attraction with $PtCl_6^{2-}$ (the precursor of PtNPs) with opposite charges facilitates the good dispersion of PtNPs.

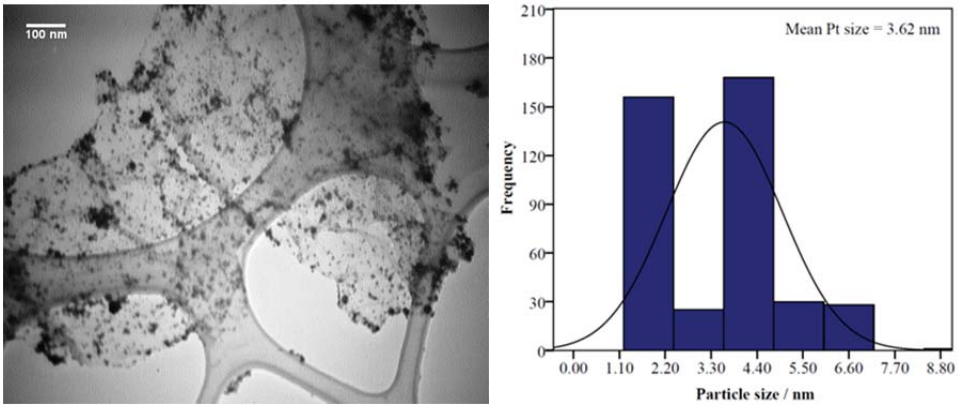

Fig. 1. TEM image of Pt/MV-RGO-CH catalyst

3.2. Methanol oxidation reaction (MOR)

The electrocatalytic performance of Pt/MV-RGO-CH catalyst is investigated towards methanol electrooxidation through cyclic voltammetry (CV) in 0.5 M H_2SO_4 and 1.54 M methanol at 34 ˚C and the scan rate of 100 mV/s[1] (Fig. 2b).

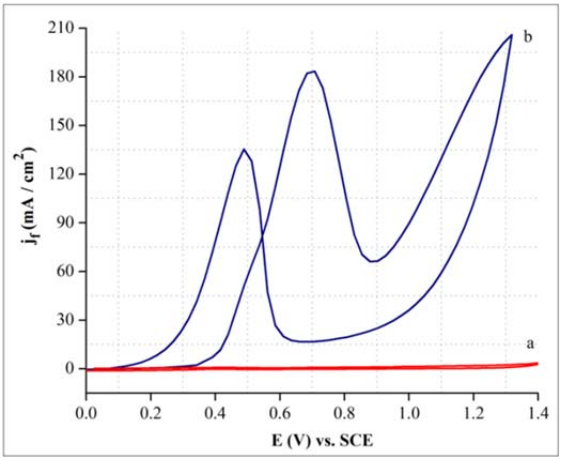

Fig. 2. CVs of a) GC/MV-RGO-CH and b) GC/Pt/MV-RGO-CH in 0.5 M H_2SO_4 and 1.54 M methanol at 34 ˚C and the scan rate of 100 mV/s[1]

As no current peak of MOR is observed in the CV curve of GC/MV-RGO-CH electrode (Fig. 2a), this electrode showed no catalytic activity for MOR (CVs at GC/CH and GC/MV-RGO electrodes are not shown, which are similar to that of GC/MV-RGO-CH electrode). The CV curve of Pt/MV-RGO-CH (Fig. 2b) catalyst showed two oxidation peaks for MOR. The

first anodic oxidation peak is observed in the forward scan around 0.71 V (E_f) which is attributed to methanol electrooxidation. The first anodic peak current density (j_f) for MOR at Pt/MV-RGO-CH catalyst was 183.48 mA/cm^2. The second oxidation peak is observed in the backward scan around 0.48 V (E_b). This peak is due to oxidation of the corresponding intermediates produced during methanol electrooxidation [30]. The second peak current density in the backward scan (j_b) was 135.45 mA/cm^2 (j_f/j_b = 1.35).

Several parameters such as methanol concentration and temperature influence the catalytic performance of Pt/MV-RGO-CH catalyst for MOR. Hence, these parameters are investigated and optimized. The effect of methanol concentration on the anodic current density of MOR on Pt/MV-RGO-CH catalyst at 34 ˚C is investigated in Fig. 3A. As shown in Fig. 3A, the anodic current density of MOR increases with increase in methanol concentration and levels off at concentrations higher than 1.54 M. This is probably due to saturation of active sites on the electrode surface. As methanol concentration increases from 0.4 to 1.54 M at Pt/MV-RGO-CH catalyst, E_f shifts towards positive direction from 0.61 to 0.71 V. This is probably due to the increase in the poisoning rate of Pt nanocatalyst. This means that the oxidative removal of the strongly adsorbed intermediates occurs at more positive potentials [31].

To study the effect of temperature on the catalytic performance of Pt/MV-RGO-CH nanocatalyst for MOR, the catalytic activity of GC/Pt/MV-RGO-CH electrode is investigated in 0.5 M H_2SO_4 and 0.79 M methanol and different temperatures ranging from 24 to 44 ˚C (Fig. 3B). As the temperature increased from 24 to 44 ˚C, j_f increased from 37.05 to 233.5 mA/cm^2. At the same methanol concentration (0.79 M methanol), the higher current density at the higher temperature reveals that there are more available Pt active sites for electrochemical reaction in the fine structure of catalyst.

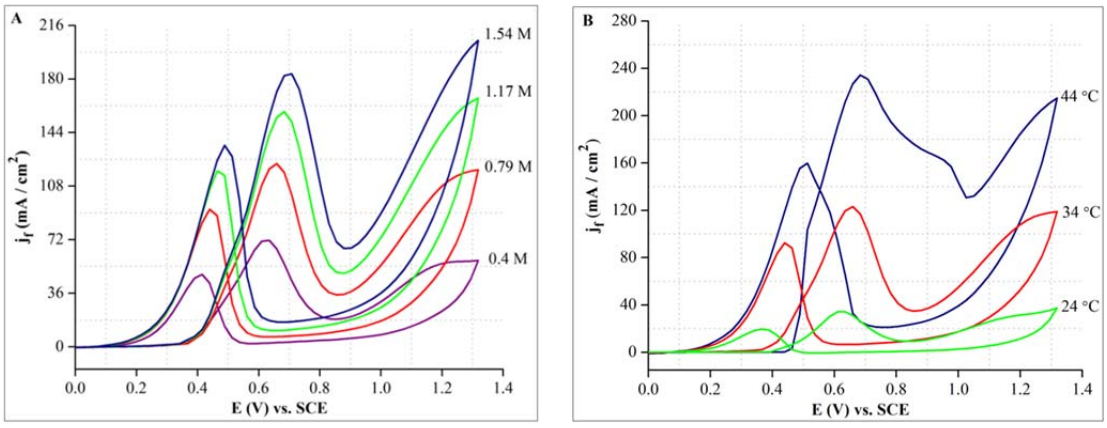

Fig. 3. A) CVs of Pt/MV-RGO-CH at 34 ˚C in 0.5 M H_2SO_4 and different concentrations of methanol: 0.4, 0.79, 1.17 and 1.54 M; B) CVs of Pt/MV-RGO-CH in 0.5 M H_2SO_4 and 0.79 M methanol at different temperature: 24, 34, and 44 ˚C

3.4. Statistical analysis using design of experiments

Investigation of the statistical analysis using DOE is a practical technique which is extensively applied to study the influence of the main factors and their combined effects on the studied responses [32, 33]. For this purpose, the Fisher's F distribution (based on the hypothesis test at 5% level of probability) is exerted for specification the significant difference among the experimental design points. The hypothesis test can be represented as below [34]:

H_0: $\mu_1 = \mu_2$ Null hypothesis
H_1: $\mu_1 \neq \mu_2$ Alternative hypothesis

The deviance of each factor at two different levels for example level 1 and level 2 is distinguished as μ_1 and μ_2. Based on the alternative hypothesis in this test ($\mu_1 \neq \mu_2$), the alteration of each main factor level leads to the significant difference in the studied response. Therefore, in the present study, temperature (at three levels, 24, 34 and 44˚C) and methanol concentration (at four levels, 0.4, 0.79, 1.17 and 1.54 M) are considered as main factors. The influence of the studied main factors and their combined effects on the anodic current density of MO is investigated according to the analysis of variance (ANOVA) test via DOE (Design-Expert version 6.0.2). Investigation of the significant difference among different levels of the factors on the anodic current density of MO at α=0.05 is carried out using Duncan's multiple range test via MSTATC software (Ver. 1.42).

3.4.1. ANOVA study of the anodic current density of MOR

ANOVA table for anodic current density of MO is presented in Table 1. Based on this Table, it is clear that both of the main factors (A: temperature and B: concentration) and their interactions (A-B) have a significant effect on the anodic current density of MO, at 5% level of probability (P-value<0.05). Meanwhile, it can be observed that the degree of freedom (Df) of temperature, methanol concentration and their interactions are equal to 2, 3 and 6, respectively. However, Df of Lack of fit as a statistical parameter is zero. Therefore, the Lack of fit is considered as insignificant parameter. It means that there is not insignificant factor (such as main factor and their interaction) in the proposed models [35,36]. Hence, Df of the proposed model is equal to 11 (the sum of Df for all of the main factors and their interactions). As can be seen in Table 1, the proposed model is significant for anticipation of the anodic current density of MO at all of the experimental conditions. The contribution of the each main factor and their interactions in the proposed model can be distinguished using F Value. Practically, the more significant factors have higher F Value and contribution percent in the proposed model [32,37]. According to Table 1, it is clear that the F Value of A, B and A-B are equal to 1159.87, 252.99 and 33.99, respectively. Therefore, it can be

deducted that the importance of factor A is higher than that of B and A-B. Meanwhile, the contribution percent of the main factors and their interactions, which are presented in Table 1, justify the obtained results of the F Value. According to Table 1, it can be observed that the contribution percent of A, B and A-B are equal to 70.15, 22.95 and 6.17, respectively. The anodic peak of MOR and its current density at Pt/MV-RGO-CH catalyst is due to methanol oxidation on Pt nanoparticles. With increase in methanol concentration, more amounts of methanol can be oxidized at the Pt surface and the anodic current density increases. This increase happens until saturation of the active sites on the electrode surface [2]. Also anodic current of MO increases with increase in temperature. The higher current density at the higher temperature reveals that there are more available Pt active sites for electrochemical reaction in the fine structure of catalyst. Also, increasing the anodic peak current densities of MOR with increase in temperature can be attributed to the fact that MOR is thermally activated. This is in reasonable agreement with the literature results for Pt catalysts [38, 39]. As mentioned, the effect of temperature on the anodic current density of methanol oxidation is more than methanol concentration. This shows that the latter mentioned reason is more remarkable.

Table 1. Analysis of variance for anodic current density of MO

Source	**Df**	**SS_{effect}**	**F Value**	**P-value**	**% Contribution**	
Model	11	3.231E+005	298.42	<0.0001	----	significant
Temperature (A)	2	2.283E+005	1159.87	<0.0001	70.15	significant
Concentration (B)	3	74697.27	252.99	<0.0001	22.95	significant
AB	6	20069.49	33.99	<0.0001	6.17	significant
Lack of fit	0	0	----	----	0.00	insignificant
Pure error	24	2362.09	----	----	0.73	----
Total	35	3.254E+005	----	----	----	----

The proposed model based on the analysis of variance is presented in Table 2. As can be seen, the proposed model includes the significant main factors and their interactions. In addition, it is clear that the coefficients of temperature (A) are higher than that of concentration (B) and their interactions (A-B). According to the listed statistical parameters, the adequacy of the proposed model can be confirmed. The most conventional statistical parameter, which can be applied for adequacy investigation of the model, is the coefficient of determination (R^2). Based on the presented results in Table 2, it is clear that the value of R^2 for the proposed model is 0.9927. According to this value, it can confirm that up to >99%, the variation of the anodic current density of MO is predictable using this model. Therewith, the adequacy of the proposed model can be validated using the adjusted R-Squared (R^2_{adj}). The comparison between the values of R^2 and R^2_{adj} can be applied for verification the result of R^2

[34, 36]. As can be seen, the difference between the values of R^2 and R^2_{adj} is equal to 0.003 which is negligible. Therefore, it can be deducted that the proposed model contains only the significant factors. Thus, the proposed model has reasonable adequacy for prediction of the studied response.

Table 2. The proposed model for anodic current density of MO and statistical parameters

Final Equation in Terms of Coded Factors	$j_f = 133.21 - 96A - 2.99A^2 - 69.99B - 7.64B^2 + 26B^3 + 43.32AB + 6.88A^2B + 0.44AB^2 - 3.20A^2B^2 - 15.71AB^3 - 2.48A^2B^3$	
Statistical parameters	R-Squared (R^2)	0.9927
	Adj R-Squared(R^2_{adj})	0.9894

3.5. The adequacy investigation of the model via graphical method

According to the obtained results of the analysis of variance, it concludes that the proposed model can strictly predict the anodic current density of MO. The obtained results are acceptable if the assumptions of the analysis of variance test be confirmed. Some of these assumptions are normality and independently of errors [34,40].

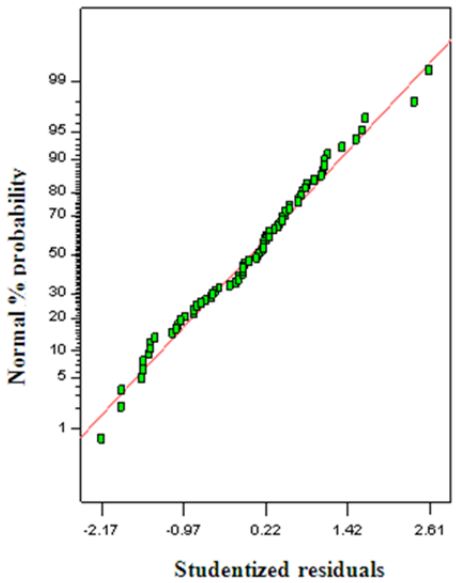

Fig. 4. Normal probability plot of residuals for anodic current density of MO

Graphical method is an applicable technique that can be used for investigation of the normality and independency of errors. Normal probability plot of residuals can be applied for investigation of the normal distribution of errors. Fig. 4 illustrates the normal probability plot of residuals for anodic current density of MO. According to Fig. 4, it is clear that the obtained

error in the ANOVA test has normal distribution. Therefore, the first assumption of the ANOVA test verifies. Thus, the proposed model has sufficient adequacy for prediction of the anodic current density of MO at the studied levels of factors.

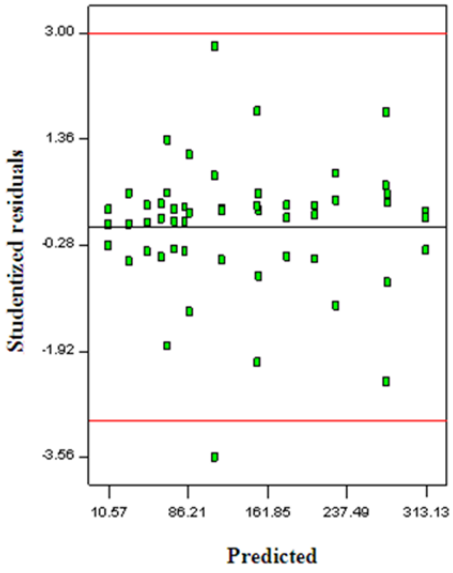

Fig. 5. Studentized residual versus predicted plot for anodic current density of MO

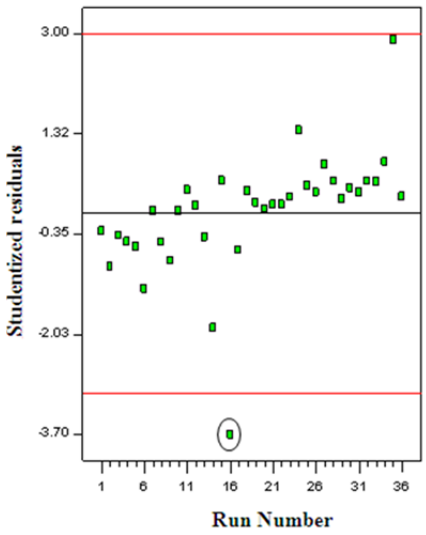

Fig. 6. Outlier t plot of residuals for anodic current density of MO

The studentized residual versus predicted plot for anodic current density of MO is presented in Fig. 5. Based on this Fig., it can be observed that there is no special pattern between studentized residuals and predicted values. Therefore, the second assumption of ANOVA test can be verified according to the results of Fig. 5. The perturbation between studentized residuals and run number can be evaluated using the outlier test. According to this graphical test, the number of the outlier design points can be recognized [34]. Increasing the number of the outlier design points in this graphical test is not reasonable. The presence

of these points can be due to the absence of the sufficient accuracy in the experimental procedure. Fig. 6 depicts the outlier t plot of residuals for anodic current density of MO. As can be observed, the number of the outlier design point is one. Therefore, it can be said that this point cannot threat the accuracy of the proposed model. Thus, this graphical test can justify the obtained results of the ANOVA test.

The quantitative results obtained based on the statistical parameters confirm that the proposed model can predict the variation of the anodic current density of MO with high accuracy. The graphical comparison between the actual and predicted values of the anodic current density of MO is presented in Fig. 7. According to this Fig., it is clear that the experimental results are equal to the predicted values using the proposed model. Therefore, the graphical method emphasizes the quantitative results.

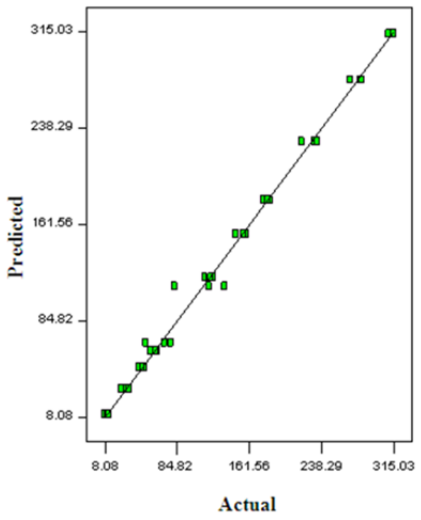

Fig. 7 Predicted versus actual values for anodic current density of MO.

3.6. A-B interaction study

The interaction between temperature and concentration as main factors is illustrated in Fig. 8. Based on Fig. 8, it can be observed that the anodic current density of MO increases with respect to the temperature (ranging from 24˚C to 44˚C) and methanol concentration (ranging from 0.4 M to 1.54 M). According to the slope of the potted lines in this Fig., it can be said that these lines are not parallel together. Therefore, the influence of temperature on methanol concentration and vice versa is reasonable and significant. The results of the analysis of variance justify these results. Thus, the proposed model can contain the main factors and mutual interaction among them for prediction of the anodic current density of MO.

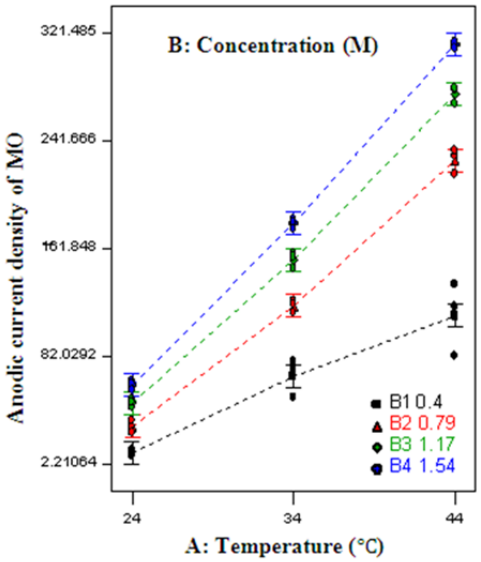

Fig. 8 Two factor interaction plots for anodic current density of MO

3.7. Main factor levels

The effect of different levels of the main factors can be investigated according to the Duncan's multiple range test [41].

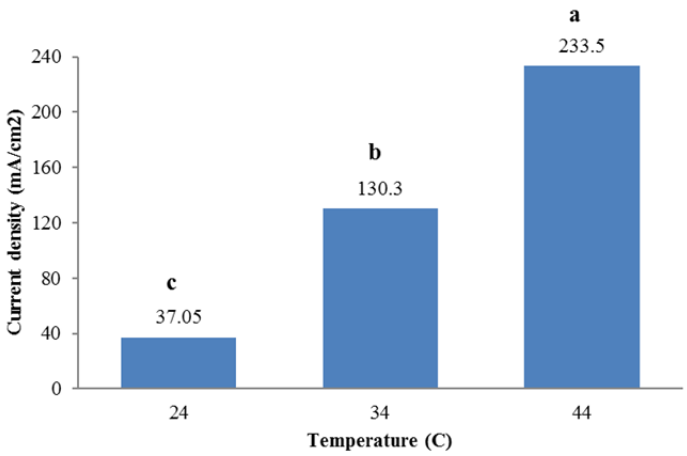

Fig. 9. Influence of the temperature on the anodic current density of MO, (The presence of the different letters on each column depicts the significant difference based on Duncan's multiple range test at α=0.05)

The influence of temperature (24, 34 and 44˚C) on the anodic current density of MO in 0.79 M methanol and 0.5 M H_2SO_4 solution is shown in Fig. 9. Based on this Fig., it is clear that according to the Duncan's multiple range test (α=0.05), there is a significant difference among three levels of the studied temperature. Meanwhile, it is confirmed that the minimum (37.02 mA/cm^2) and maximum (233.5 mA/cm^2) anodic current density of MO are recorded for the temperature of 24 ˚C and 44 ˚C, respectively. Therefore, the enhancement of the

anodic current density of MO during the increment of the temperature from 24˚Cto 44 ˚C is equal to 530.22%.

The influence of methanol concentration on the anodic current density of MO at 34 ˚C is presented in Fig. 10. It is clear that there is a reasonable difference between four methanol concentrations on the anodic current density of MO according to the Duncan's multiple range test at α=0.05. Meanwhile, by increasing the methanol concentration from 0.4 M to 1.54 M, the anodic current density of MO increases. Index increases from 0.4 M (64.9 mA/cm^2) to 0.79 M (125.6 mA/cm^2) is equal to 93.52%; from 0.79 M to 1.17 M (159 mA/cm^2) is equal to 2.59% and from 1.17 M to 1.54 M (184.9 mA/cm^2) is equal to 16.28%. In addition, with increase in methanol concentration from 0.4 M to 1.54 M, the anodic current density of MO enhances 184.89%. Therefore, comparing the influence of the temperature with methanol concentration reveals that the effect of temperature (530.22%) is more significant than that of methanol concentration (184.89%).

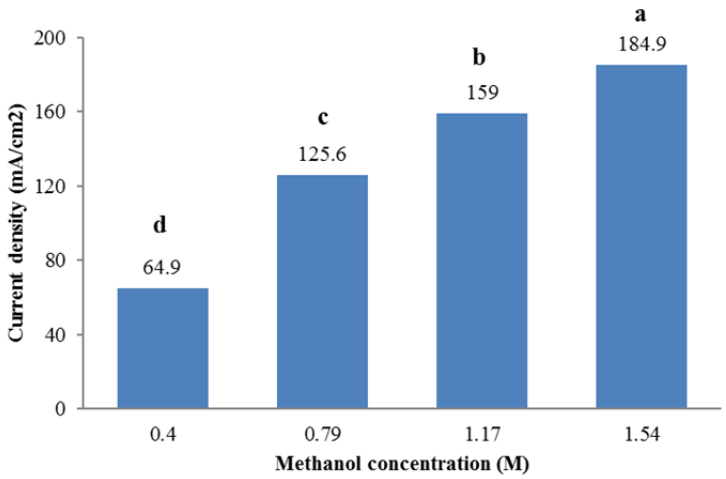

Fig. 10. Influence of methanol concentration on the anodic current density of MO, (The presence of the different letters on each column depicts the significant difference based on Duncan's multiple range test at α=0.05)

4. CONCLUSION

Herein, we investigate the effect of the interaction between temperature and methanol concentration on the anodic current density of MO using design of experiments and Duncan's multiple range tests. The results show that anodic current density of MO increases with increase in temperature and methanol concentration. Meanwhile, the statistical analysis confirms that all of the studied factors can significantly affect the response. The results of the analysis of variance reveals that the proposed models, which contains the both main factors and their interaction, can predict the response at any level of factors. The graphical methods justify the adequacy of the proposed model. The results of the Duncan's multiple range test

reveals that there is a significant difference among different levels of temperature and methanol concentration.

Acknowledgements

The authors hearty thank from Esfarayen University of Technology.

REFERENCE

[1] M. S. Ekrami-Kakhki, Z. Yavari, J. Saffari, and S. Abbasi, J Nanostruct 6 (2016) 221.
[2] M. Noroozifar, M. Khorasani-Motlagh, M. S. Ekrami-Kakhki, and R. Khaleghian-Moghadam, J. Power Sources 248 (2014) 130.
[3] J. N. Tiwari, R. N. Tiwari, G. Singh, and K. S. Kim, Nano Energy 2 (2013) 553.
[4] X. Zhou, Y. Gan, J. Du, D. Tian, R. Zhang, C. Yang, and Z. Dai, J. Power Sources 232 (2013) 310.
[5] S. L. Gojkovic, T. Vidakovic, and D. Đurovic, Electrochim. Acta 48 (2003) 3607.
[6] S. Kim, M. H. Cho, J. R. Lee, and S. J. Park, J. Power Sources 159 (2006) 46.
[7] Z. Q. Tian, S. P. Jiang, Y. M. Liang, and P. K. Shen, J. Phys. Chem. B 110 (2006) 5343.
[8] H. D. Du, B. H. Li, F. Y. Kang, R. W. Fu, and Y. Q. Zeng, Carbon 45 (2007) 429.
[9] D. A. Konopka, M. Li, K. Artyushkova, N. Marinkovic, K. Sasaki, R. Adzic, T. L. Ward, and P. Atanassov, J. Phys. Chem. C 115 (2011) 3043.
[10] B. Fang, M. Kim, and J. S. Yu, Appl. Catal., B: Environ. 84 (2008) 100.
[11] Y. Fang, D. Zhang, X. Qin, Z. Miao, S. Takahashi, J. I. Anzai, and Q. Chen, Electrochim. Acta 70 (2012) 266.
[12] J. Lobato, P. Canizares, D. Ubeda, F. J. Pinar, and M. A. Rodrigo, Appl. Catal., B: Environ. 106 (2011) 174.
[13] S. S. John, I. Dutta, and A. P. Angelopoulos, Langmuir 27 (2011) 5781.
[14] J. Qi, L. Jiang, S. Wang, and G. Sun, Appl. Catal., B: Environ. 107 (2011) 95.
[15] H. Zhang, X. Xu, P. Gu, C. Li, P. Wu, and C. Cai, Electrochim. Acta 56 (2011) 7064.
[16] Y. Zhang, C. Liu, Y. Min, X. Qi, and X. Ben, J. Mater. Sci. Mater. Electron. 24 (2013) 3244.
[17] Z. K. Ghouri, N. A. M. Barakat, P. S. Saud, M. Park, B. S. Kim, and H. Y. Kim, J. Mater. Sci. Mater. Electron. 27 (2016) 3894.
[18] Y. Li, L. Han, B. An, Y. Wang, L. Wang, X. Yin, and J. Lu, J. Mater. Sci. Mater. Electron. 27 (2016) 6208.
[19] K. Kakaei, and H. Gharibi, Energy 65 (2014) 166.
[20] S. Han, D. Wu, S. Li, F. Zhang, and X. Feng, Adv. Mater. 26 (2014) 849.
[21] Y. Li, and L. T. J. Li, Electrochem. Commun 11 (2009) 846.

[22] F. Jafari, A. Salimi, and A. Navaee, Electroanalysis 26 (2014) 1782.
[23] J. Zhao, H. Yu, Z. Liu, M. Ji, L. Zhang, and G. Sun, J. Phys. Chem. C 118 (2014) 1182.
[24] S. Guo, S. Dong, and E. Wang, ACS Nano 4 (2009) 547.
[25] S. Mayavan, H. S. Jang, M. J. Lee, S. H. Choi, and S. M. Choi, J. Mater. Chem. A 1 (2013) 3489.
[26] J. Ma, L. Wang, X. Mu, and Y. Cao, J. Colloid Interface Sci. 457 (2015) 102.
[27] M. Khorasani-Motlagh, M. Noroozifar, and M. S. Ekrami-Kakhki, Int. J. Hydrogen Energy 36 (2011) 11554.
[28] J. Ma, L. Wang, X. Mu, and L. Li, Int. J. Hydrogen Energy 40 (2015) 2641.
[29] P. Zeng, R. Ran, Z. Chen, W. Zhou, H. Gu, Z. Shao, and S. Liu, J. Alloys Compd. 455 (2008) 465.
[30] M.-S. Ekrami-Kakhki, M. Khorasani-Motlagh, and M. Noroozifar, J. Appl. Electrochem. 41 (2011) 527.
[31] Z. He, J. Chen, D. Liu, H. Zhou, and Y. Kuang, Diamond Relat. Mater 13 (2004) 1764.
[32] S. Abbasi, and M. Hasanpour, J. Mater. Sci. Mater. Electron. 28 (2017) 1307.
[33] N. Roozban, S. Abbasi, and M. Ghazizadeh, J. Mater. Sci. Mater. Electron. 28 (2017) 6047.
[34] S. Abbasi, M. Hasanpour, and M. S. E. Kakhki, J. Mater. Sci. Mater. Electron 28 (2017) 9900.
[35] M. Namvar-Mahboub, and M. Pakizeh, Korean J. Chem. Eng. 31 (2014) 327.
[36] N. Roozban, S. Abbasi, and M. Ghazizadeh, J. Mater. Sci. Mater. Electron 28 (2017) 7343.
[37] A. Kazemi-Beydokhti, H. A. Namaghi, M. A. H. Asgarkhani, and S. Z. Heris, Braz. J. Chem. Eng. 32 (2015) 903
[38] O. Sahin, and H. A. Kivrak, Int. J. Hydrogen Energy 38 (2013) 901.
[39] A. V. Tripkovic, K. D. Popovic, B. N. Grgur, B. Blizanac, P. N. Ross, and N. M. Markovic, Electrochim. Acta 47 (2002) 3707.
[40] A. Ahmad, M. I. Ahmad, M. Younas, H. Khan, and M. U. H. Shah, Iran J. Chem. Chem. Eng. 32 (2013) 33.
[41] S. Abbasi, S. M. Zebarjad, S. H. N. Baghban, and A. Youssefi, Bull. Mater. Sci. 37 (2014) 1439.